

Atomistic study of energy funneling in the light-harvesting complex of green sulfur bacteria

Joonsuk Huh,^{1,*} Semion K. Saikin,¹ Jennifer C. Brookes,^{1,2}
Stéphanie Valteau,¹ Takatoshi Fujita,¹ and Alán Aspuru-Guzik^{1,†}

¹*Department of Chemistry and Chemical Biology,
Harvard University, Cambridge, Massachusetts 02138, United States*

²*Department of Physics and Astronomy, University College London, Gower, London WC1E 6BT*

Phototrophic organisms such as plants, photosynthetic bacteria and algae use microscopic complexes of pigment molecules to absorb sunlight. Within the light-harvesting complexes, which frequently have several functional and structural subunits, the energy is transferred in the form of molecular excitations with very high efficiency. Green sulfur bacteria are considered to be amongst the most efficient light-harvesting organisms. Despite multiple experimental and theoretical studies of these bacteria the physical origin of the efficient and robust energy transfer in their light-harvesting complexes is not well understood. To study excitation dynamics at the systems level we introduce an atomistic model that mimics a complete light-harvesting apparatus of green sulfur bacteria. The model contains approximately 4000 pigment molecules and comprises a double wall roll for the chlorosome, a baseplate and six Fenna-Matthews-Olson trimer complexes. We show that the fast relaxation within functional subunits combined with the transfer between collective excited states of pigments can result in robust energy funneling. Energy transfer is robust on the initial excitation conditions and temperature changes. Moreover, the same mechanism describes the coexistence of multiple timescales of excitation dynamics frequently observed in ultrafast optical experiments. While our findings support the hypothesis of supertransfer, the model reveals energy transport through multiple channels on different length scales.

I. INTRODUCTION

Photosynthetic bacteria are among the simplest organisms on Earth which use sunlight as their main energy source [1]. To collect solar energy these bacteria exploit light-harvesting complexes (LHC), aggregates of pigment molecules, which absorb photons and transfer the associated energy at the submicron scale. The LHC in green sulfur bacteria contains large light absorbing antennae self-assembled in the so-called chlorosome [2]. These bacteria are obligate phototrophs – they are required to use sunlight to support metabolic reactions [3–5]. However, it has been observed that green sulfur bacteria can live in extremely low light conditions, even when receiving only a few hundred photons *per bacterium* per second [6–8]. These facts have inspired many conjectures and discussions on the functional properties, energy conversion efficiency and robustness of LHC in green sulfur bacteria [9–15].

In order to address this controversy we introduce a model which includes atomistic structural detail of the green bacteria LHC and allows for the simulation of excitation energy transfer (EET) at the systems level. As a specific example, we consider the LHC of *Chlorobium tepidum*. We observe fast relaxation of excitations within the subunits of LHC owing to the large overlap between exciton states and strong interaction with environmental fluctuations. The transfer between subunits involves collective excited states of the pigment

molecules and supports the hypothesis of supertransfer [12, 14, 15]. The energy transport is robust to different initial excitation conditions, and changes in temperature. Finally, we show that the population of different parts of the LHC can be described using simple kinetic equations with time-dependent transfer rates characterizing intra-unit dynamics. This later model naturally explains the multiple timescales of EET reported in optical studies of green sulfur bacteria [16–20] and green non-sulfur bacteria [21–23].

Theoretical models have been applied mostly to single functional units of LHCs [24–32] in order to understand the physical principles of energy transfer. Some of these studies also involved atomistic structures [30, 32–34], which make the models computationally demanding. To the authors knowledge there are only a few atomistic studies of the complete light-harvesting systems of purple bacteria [35, 36] but none for green sulfur bacteria. In addition to the large scale calculations the detailed analysis of excitation dynamics on the systems level [23, 35–38] is complicated due to the lack of structural information. Thus, one usually needs to use macroscopic phenomenological models [39] or introduce additional constraints and approximations on the transport models [40, 41].

The LHC in green sulfur bacteria is composed of bacteriochlorophyll (BChl) pigment molecules. These monomers aggregate in several interconnected functional units, as shown in Fig. 1A. The main element of LHC is the chlorosome – an ellipsoidal shaped body of size ranging from tens to hundreds of nanometers [2]. The chlorosome is densely packed with BChl *c* pigments. Two other functional units – the baseplate [42] and the Fenna-Matthews-Olson (FMO) trimer complex [43] are com-

* Email: huh@fas.harvard.edu

† Email: aspuru@chemistry.harvard.edu

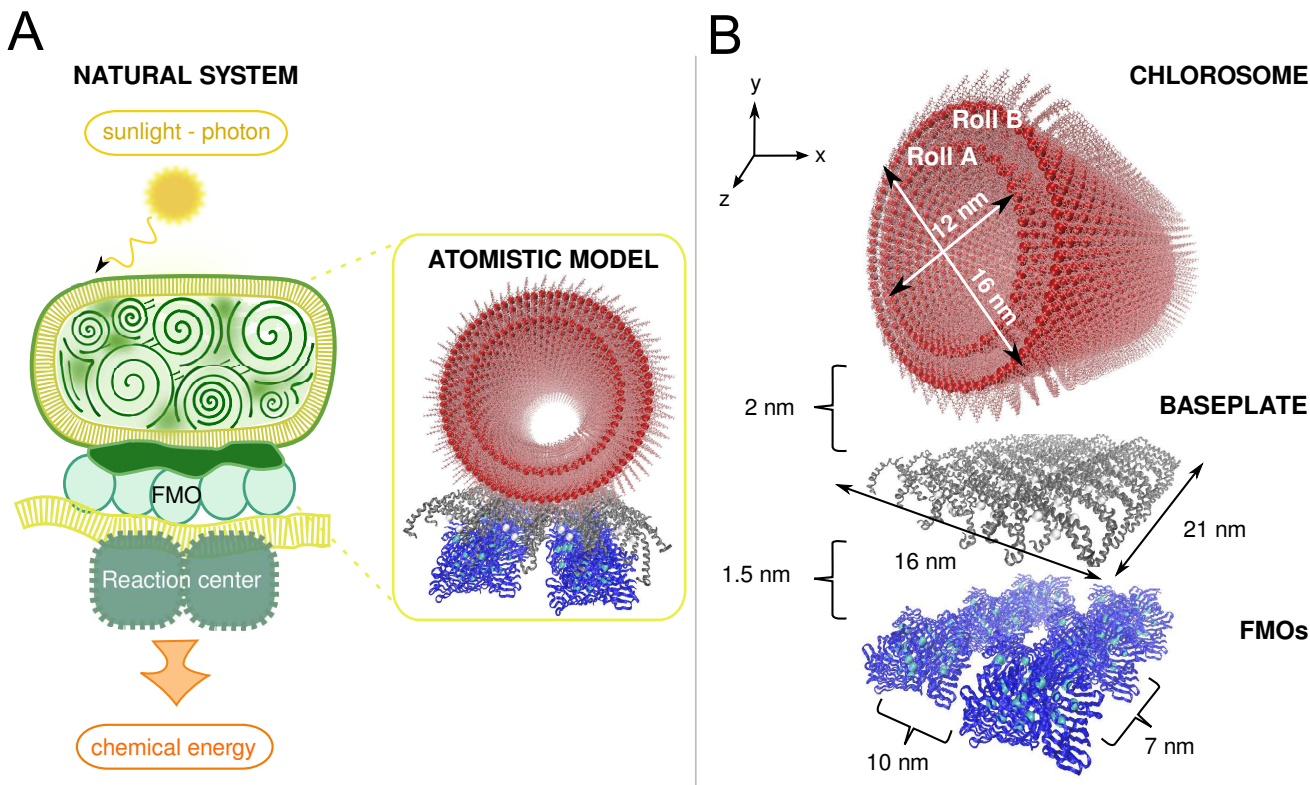


Figure 1. **Photosynthetic apparatus.** **A**, Cartoon of light-harvesting complex in green sulfur bacteria. The bacteria transform solar photons into chemical energy. Sunlight absorbed by the chlorosome is transferred in the form of an exciton through the baseplate and Fenna-Matthews-Olson (FMO) complexes subsequently to the reaction center. A snapshot of the model structure is also shown. **B**, Atomistic model with corresponding length scales. The atomistic model is composed of a double wall roll for the chlorosome (Roll A: 1620 ($=60 \times 27$) BChl *c* sites and Roll B: 2160 ($=80 \times 27$) BChl *c* sites), baseplate (64 BChl *a* sites) and 6 FMO trimer complexes (144 ($=24 \times 6$) BChl *a* sites).

posed of BChl *a* pigments held together by a protein scaffolding. Energy in the form of molecular excitations (*i.e.* exciton) is collected by the chlorosome and funneled through these antenna units to the reaction center where charge carriers are then generated. The distance between the pigments in LHCs is sufficiently large such that the overlap of electronic wave functions can be neglected. In this case the energy transfer is mediated by the near field interaction between molecular electronic transitions, the Förster interaction [44–46]. If the interaction between several molecules is sufficiently strong as compared to the energy difference between their electronic transitions, the exciton states are delocalized over the group of pigments [45, 46]. The preferential direction for energy transport is controlled by the frequencies of electronic transitions: the excitation goes to molecules or groups of molecules with lower excited state energy, while dissipating the energy difference to the environment.

A. Molecular aggregate model

A single LHC of *Chlorobium tepidum* contains 200–250 thousand BChl molecules [2, 19, 47]. Most of these molecules are found in the chlorosome. The model we have created is shown in Fig. 1, it is composed of 3988 pigments and represents all the functional units of LHC in green sulfur bacteria, excluding the reaction center.

In our model (Fig. 1B) a double wall roll aggregate with diameter of about 16 nm and length of about 21 nm, represents the chlorosome. Several possible structural arrangements of BChls in the chlorosome have been investigated theoretically and experimentally [48–54]. Here we use the structure of Ref. [52], obtained from a triple mutant bacteria and characterized with nuclear magnetic resonance and cryo-electron microscopy. This structure is also supported by 2-dimensional polarization fluorescence microscopy experiments [55].

The microscopic structure of the baseplate has not yet been experimentally verified [42]. We construct a baseplate lattice as following. The unit cell consists of dimers of CsmA proteins [56] containing 2 BChl *a* molecules sandwiched between the hydrophobic regions and bound near the histidine. To establish a stable structure of the

baseplate, classical molecular dynamics simulations were done.¹ The final structure complies with the periodicity and dimensions of the unit cell as seen in freeze frame fracture [59]. The lattice model for the baseplate is described in the Appendix. Finally, for the FMO protein complexes we employ the structure resolved in Ref. [60].

The constructed model of the light-harvesting apparatus contains 95 % of BChl *c* and 5 % of BChl *a*, which is comparable to the stoichiometry of the natural system (99 % and 1 %) [19]. The estimated density of FMO complexes is about 1 FMO/50 nm² [61]. Therefore, we distribute 6 FMO complexes under the baseplate which occupies about 300 nm² (see Fig. 1B). This gives a pigment ratio of 2.3:1 (FMOs:baseplate), which is similar to the corresponding stoichiometry of *Chlorobium tepidum* 2:1 [47].

The distances between the chlorosome BChl *c* aggregates and the baseplate is determined by the length of BChl *c* esterifying alcohols. In the case of *Chlorobium tepidum* it is about 2 nanometers [20, 23, 42]. While the orientation of FMO relative to the baseplate has been verified experimentally [61], the relative distance between these units is unknown. In our model we set it to be 1.5 nm, which is larger than the inter-pigment distance within FMO but smaller than the baseplate-chlorosome distance. This choice is based on the argument that the FMO complex is strongly linked to the baseplate [62]. Minor variations of this distance do not affect the results.

The frequencies of exciton transitions in LHCs are controlled by multiple factors. In the model it is equivalent to use the relative shifts (energy gap) of these transitions, which are relevant to the EET. These shifts can be calculated from the pigment-pigment couplings and the electronic excitations of single BChls, site energies, modified by the local environment [63]. While the couplings can straightforwardly be computed using a screened dipole-dipole model [63], the calculation of site energies requires more complicated models or fitting to experimentally measured optical spectra. Here, we set the frequency offset to be aligned with the lowest site energy of the FMO complex [62, 64].

The absorption domains of the baseplate and FMO composed of BChl *a* pigments are not clearly distinguishable. The absorption band of the baseplate covers the range 790–810 nm. This range also includes the absorption band of the FMO complexes [20, 64, 65]. In fact, the absorption band of the baseplate significantly overlaps with that of the chlorosome [20]. In order to reproduce these spectra using the constructed model we define the site energy of BChl *c* to be 2950 cm⁻¹, which places the absorption maximum of the chlorosome of about 640 cm⁻¹ above the absorption maximum of FMO

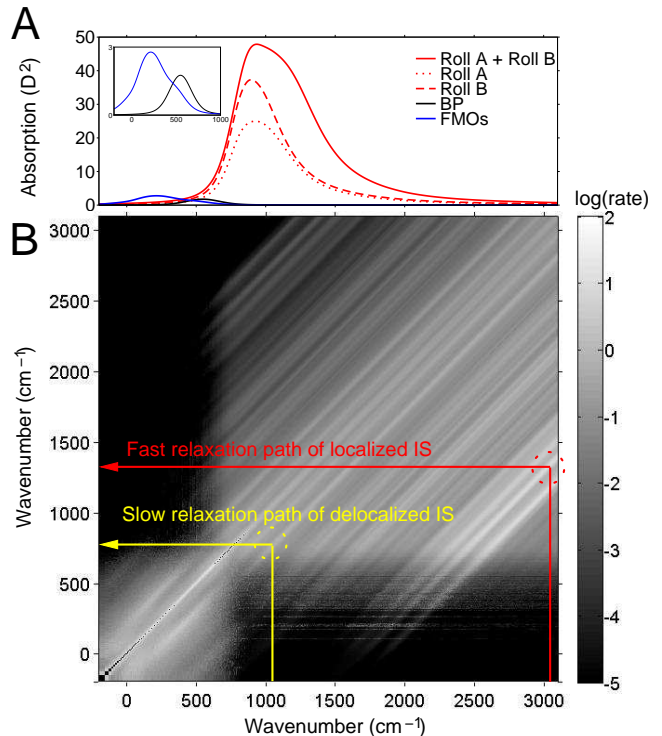


Figure 2. Calculated absorption spectra and exciton transfer rate matrix γ_{MN} . **A**, Calculated absorption spectra [67] by direct diagonalization of the system Hamiltonians of the antenna units in Fig. 2 are shown. The absorption spectra are calculated and drawn for the double wall roll (Roll A + Roll B), the single rolls (Roll A and Roll B), the baseplate and the 6 FMO complexes. The absorption spectrum of each antenna unit is obtained after taking 1000 ensemble average over the site energy fluctuations (static disorder). A Lorentzian line shape function with a full width at half maximum of 100 cm⁻¹ is convoluted, additionally, to take the homogeneous broadening into account. **B**, Transfer rate matrix γ_{MN} (cm⁻¹) at 300 K is presented in a logarithmic scale. γ_{MN} indicates population transfer rate between exciton states $|M\rangle$ and $|N\rangle$. We set, here, the frequency offset to be aligned with the lowest site energy of the FMO complex.

complexes (see Fig. 2A). Our choice is based on the fluorescence maximum of the chlorosome (786 nm) [20]. We shift the lowest exciton state obtained after taking 1000 ensemble average over the site energy fluctuation (standard deviation: 500 cm⁻¹ [66]) at the fluorescence maximum. 12225 cm⁻¹ (818 nm) is used as the offset energy value. We assign the site energy of the baseplate as 550 cm⁻¹, which places the absorption maximum of the baseplate approximately in the middle of the absorption maxima of the FMO complexes and the chlorosome. The resulting absorption spectrum of the baseplate is shown in Fig. 2A.

¹ The NAMD program package version 2.8 [57] was used. Force fields were parameterized with a combination of Amber ff99SB for the protein [58] and MMFF94 atomic charges for the BChl *a*.

B. Exciton transfer model

The exciton transfer is modelled with a quantum master equation approach, which includes the coherent, dephasing and relaxation processes, for the open quantum dynamics [63, 68–71]. We solve the quantum master equation to obtain the spacial distribution of the exciton.

In our model, the system-bath Hamiltonian of the light-harvesting apparatus is composed of three parts: the system consists of the local excitations of bacteriochlorophylls (BChls) and the point dipole interactions between them, described using a tight-binding Hamiltonian. Then, the system (BChls) is coupled linearly to the bath (proteins). The bath Hamiltonian consists of a sum of multidimensional quantum harmonic oscillators (see *e.g.* Ref. [71] and the Appendix).

Within the secular approximation and in the Markov limit (*i.e.* secular Redfield), the equations of motion of the reduced density operator $\hat{\rho}_S(t)$ in the exciton basis, the population and coherence transfer are decoupled [72]. The equations of motion is given in the Appendix.

The resulting quantum master equation includes a term γ_{MN} , which is the exciton transition rate between the corresponding exciton states $|M\rangle$ and $|N\rangle$. γ_{MN} is calculated with the exciton eigenvectors and spectral density (exciton-phonon coupling strength) at the transition energy (see Ref. [71, 73] for the definition and also the Appendix for the expressions). It is shown in Fig. 2B as a matrix, for the EET dynamics at 300 K.

The validity of the Redfield method for the EET in natural light-harvesting structures had been discussed by many authors, see *e.g.* Refs. [72, 74–78] and the references cited therein. When the energy gap between the exciton states is small, the Redfield model with a broad spectral density can be applicable [76]. Our molecular aggregate model in Fig. 1 and the corresponding spectral densities [30, 66] satisfy this condition: the absorption spectra of the antenna units overlap each other significantly, which implies the exciton states in this energy domain are delocalized over the two antenna units. The antenna units are coupled weakly (16–17 cm^{-1}). The spectral densities and the density of states are given in the Appendix.

Novoderezhkin and *et al.* [77] proposed to compensate the underestimation of the transfer rate between exciton states with large energy gaps by increasing the spectral density in the high frequency region. Therefore, we note here the exciton transition rate, which involves the exciton transfer with a large energy gap, could be underestimated because the Redfield model can only account for the single phonon process. Multiphonon processes could occur in the internal exciton dynamics of the antenna units due to its broad exciton bands (see Fig. 2A). The internal exciton dynamics of the chlorosome is, however, much faster than the exciton transfer between the antenna units. Thus, the Redfield model should give a reasonable results (timescales) qualitatively for the exciton

funneling process of the photosynthetic apparatus. For more accurate models, one would consider other methods such as the modified Redfield approach [74, 76, 78], hierarchical equations of motion [28, 79–81], iterative linearized density matrix dynamics [82], non-Markovian quantum state diffusion [29, 83], variational master equation [84], path integral Monte Carlo [85], and see the references cited in the review [86] of the methodologies in EET. However, most of these sophisticated methods, are not applicable to our large system because they are numerically too demanding.

The effects of slow fluctuations in the site energies (static disorder), which are responsible for the inhomogeneous broadening, are incorporated. We use 100 cm^{-1} for the Gaussian fluctuations in FMO and the baseplate, and 500 cm^{-1} for the roll [64, 66]. All results are obtained from 1000 ensemble averages for the static disorder, unless otherwise mentioned.

The system Hamiltonian of FMO trimer complexes is taken from Ref. [62]. The spectral density from our previous work [30] is used: where molecular dynamics and time-dependent density functional theory calculations were used for obtaining it. A harmonic prefactor was used for the spectral density [73]. The structure of the double wall roll is obtained based on Ref. [52]. The structure was optimized with molecular dynamics simulation and a spectral density was obtained by time-dependent density functional theory calculations [66, 73].

Instead of computing the spectral density of the baseplate, which is composed of BChl *a*, we use the spectral density of FMO [30]. This approximation is justified because we expect the vibrational structure to be similar to FMO's, which is surrounded by a protein environment (*cf.* chlorosome) and is also composed of BChl *a*.

To this end, we define the mean exciton energy to quantify the energy dissipation from the system to the bath during the energy funneling process,

$$\text{MEE}(t) = \mathcal{E} \left(\text{Tr}_S \left(\hat{H}_S \hat{\rho}_S(t) \right) \right), \quad (1)$$

where \hat{H}_S is the system Hamiltonian and Tr_S is the trace over the system degrees of freedom. \mathcal{E} is the ensemble average over the static disorder.

Additionally, we introduce the cooperativity, which is used to quantify the enhancement of transition dipole moment by coherence. Cooperativity(t) can be interpreted as excitation delocalization, as following

$$\text{Cooperativity}(t) = \frac{1}{|\mu|^2} \mathcal{E} \left(\sum_{\alpha=x,y,z} \sum_{m,n \in \text{Domain}} \mu_{n,\alpha} \mu_{m,\alpha} \langle n | \hat{\rho}_S(t) | m \rangle \right), \quad (2)$$

where μ_n is the transition dipole moment vector of site n and a normalization factor $|\mu|^2 = 30 \text{ D}^2$, which is the absolute square of the transition dipole moment of a single pigment, is used. All pigments have the same magnitude of the transition dipole moment in our model (Fig. 1B).

$|m\rangle$ and $|n\rangle$ are the site basis states. The summation is over the domain of interest.

II. EXCITATION ENERGY FUNNELING

To fully characterize the exciton transfer process of the photosynthetic apparatus model in Fig. 1, one needs to study the exciton dynamics for all possible initial (exciton) states within an ensemble at a finite temperature. For instance, the initial state prepared by a coherent light source (laser) could be considered as a single exciton state [87]. As an example, we perform exciton dynamics simulations for two cases of initial excitation at 300 K to see how the initial condition affects the EET dynamics. One is the brightest exciton state of the system Hamiltonian of Roll A, which is delocalized over Roll A (see the snapshot of Fig. 3A at 0 ps) and has energy 1018 cm^{-1} . The other initial condition to be considered is a localized initial state (IS). In particular, a single site located on top and in the middle of Roll A is selected for the localized IS having energy 3022 cm^{-1} (see the snapshot of Fig. 3B at 0 ps).

Comparing the absorption spectra of Roll A and Roll B in Fig. 2A, one can see the peak maximum of Roll B is red-shifted from the peak maximum of Roll A, thus there is an exciton energy gradient between the layers. As the radius of the roll increases (contrast A and B), the peak maximum shifts to the red [21, 51, 67]. This occurs because the roll curvature changes and this induces stronger dipole-dipole interactions between neighboring pigments. This energy gradient is favorable for the exciton energy funneling because EET from the outermost layer to the baseplate is important. Our choice of the initial states on the Roll A is based on this argument.

There are two important factors in determining the exciton transfer between the antenna units. These are the energy resonance condition and the electronic coupling between the energy levels of the antenna units [88]. The former is the necessary condition for the EET between the units and the later determines how fast EET should be. Fig. 2 shows the delocalized IS is close to the energy levels of the baseplate and large multichromophoric excitonic coupling strengths to the baseplate exciton states. In contrast, the localized IS is far from the energy resonance level to the baseplate and the excitonic coupling strength is small.

Fig. 3 summarizes the resulting exciton dynamics at 300 K. Figs. 3A and 3B show the population dynamics using the delocalized IS and the localized IS respectively and up to 10 ps. Our choice of the time interval (10 ps) of the EET simulation is based on the timescales of the EET of *Chlorobium tepidum* in Ref. [20]. Snapshots of the site populations at 0 ps, 0.1 ps and 10 ps are shown below the population plots. The exciton population distributions of individual antenna units at 10 ps are almost identical regardless of the initial conditions. For example, the total exciton population on FMOs is approximately 60 % for

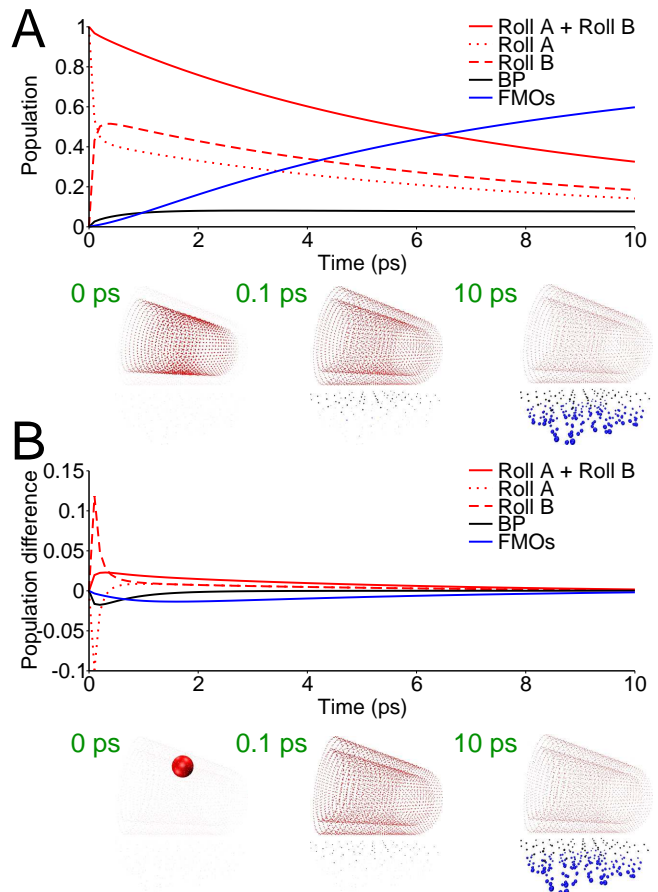


Figure 3. **Exciton population dynamics with a delocalized and a localized initial state at 300 K.** **A**, The initial state (see the snapshot at 0 ps) is the brightest state of Roll A. **B**, The initial state (see the snapshot at 0 ps) is a localized state, *i.e.* a site on the top and in the middle of the Roll A. The population difference with respect to the population in **A** are plotted. The locations of magnesium (Mg) in the BChls represent the locations of exciton sites and the sizes of the spheres are proportional to the populations of the corresponding sites. The populations of the rolls, the baseplate and the FMOs are designated red, black and blue, respectively.

the two initial conditions.

In the rest of this section, we provide more detailed discussion of severe aspects of the exciton transfer. First, the exciton population dynamics of the two initial conditions are compared. Then, the multichromophoric effect is discussed for the exciton dynamics. The temperature dependence of the exciton dynamics comes afterwards. Lastly, the exciton dynamics is described in terms of the population kinetic model.

A. Exciton population dynamics

The EET dynamics of the delocalized IS and the localized IS become similar within 1 ps (Fig. 3). The short

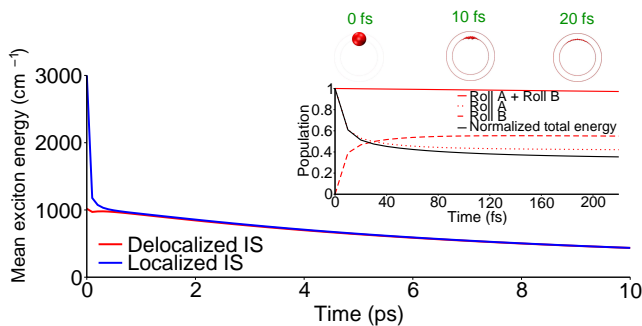


Figure 4. **Mean exciton energy with a delocalized and a localized initial state at 300 K.** Mean exciton energy (Eq. 1) with the two different initial excitations, which correspond to those in Fig. 3A and 3B. The short time dynamics for the first 200 fs of Fig. 3B is given in the inset with the corresponding population snapshots. The populations in the snapshot which are projected to the long axis of the rolls. The locations of magnesium (Mg) atoms in the BChls represent the locations of exciton sites and the sizes of the spheres are proportional to the populations of the corresponding sites.

time dynamics (< 200 fs), however, are sufficiently different. Fig. 3A shows a fast initial population decay for the roll comparing to that of the localized IS in Fig. 3B. Characteristic time constants in Table I are extracted by the exponential fitting of the exciton populations of the roll such that amplitudes are summed to be 100%. By comparing the time constants for the roll in Table I, we see that Set I (delocalized IS) has a fast sub-100-fs component while Set III (localized IS) does not. However, τ_1 in Set I accounts for only 3% of the 10 ps exciton dynamics. In the case of using the delocalized IS, the single exciton starts to migrate from the roll to the baseplate already at the very beginning (< 100 fs). This occurs because the frequency of the delocalized IS (1018 cm^{-1}) is close to the baseplate absorption region (see Fig. 2A) and has a large collective transition dipole moment.² In contrast, the localized IS (3022 cm^{-1}) is far from the energy resonant region and has a comparably weak transition dipole moment.

Equilibration in the roll is achieved within 100 fs for the localized IS dynamics and almost no exciton population is transferred to the baseplate in this short time. This can be seen in the inset figure of Fig. 4. The inset in Fig. 4 shows the diffusion process in the roll with the localized IS for the first 200 fs. Snapshots of the roll populations at 0, 10 and 20 fs are placed above the inset plot. In this plot, one can see how the single exciton diffuses within and between the layers. The black solid line in the inset figure is the mean exciton energy (Eq. 1), which is nor-

malized to the initial energy (3022 cm^{-1}). Interestingly, the curve is similar to the population dynamics of Roll A. From this we can conclude that the population transfer from Roll A to Roll B is the main energy relaxation channel and the slight difference of the two curves indicates the effect of population redistribution within the single layers. Thus the energy dissipation due to exciton-phonon coupling mainly causes exciton transfer between the layers in this initial short time period. The mean exciton energy of the total system (Roll+baseplate+FMOs) is given in Fig. 4 for two different initial excitations. The solid blue line and the solid red line correspond to the exciton dynamics of the two different initial conditions, respectively.

As mentioned above, the initial energy of the delocalized state is already close to the baseplate bright state energy domain (see Fig. 2), while that of the localized state is higher (3022 cm^{-1}). In the localized IS case, the excess energy (about 2000 cm^{-1}) should be released to the environment in order for resonant energy transfer to the baseplate to occur. In spite of the high initial energy of the localized IS, which is far from the energy resonance domain, the exciton population of each unit at 10 ps is similar to that of the delocalized IS case (see Fig. 3A). This is possible because a rapid energy relaxation channel (Fig. 2B) is available for the dynamics of Set III. The blue line in Fig. 4 shows a rapid energy drop within 100 fs, the total energy approaches the energy of the delocalized IS. The population snapshots at 100 fs indicate that population distributions are quite similar. Also, the population on the roll in the snapshots of Fig. 3B at that time indicates that, by 100 fs, the system population is mostly delocalized over the roll. The mean exciton energy obtained from the exciton dynamics with the delocalized IS and the localized IS become similar within 500 fs. The rapid relaxation within the roll results in robust energy transfer from the roll to the FMOs in the long time limit in our model study.

Microscopically, the energy dissipation dynamics is determined by thermal excitations and relaxation among exciton levels. The energy dissipation rate, in this model, depends on the spectral density, a quantity which indicates how strongly exciton states are coupled to the thermal bath, the probability distribution of the exciton states and temperature.

In Fig. 2B, we show the exciton transfer matrix (γ_{MN}) at 300 K in logarithmic scale ($\log(\text{cm}^{-1})$). We indicate the fast energy dissipation path for the localized IS with a red arrow. The strong white diagonal band corresponds to the strong exciton-phonon coupling at $1600\text{--}2000 \text{ cm}^{-1}$ [89] (see the spectral densities in the Appendix), which leads to the rapid energy dissipation of the localized IS within the roll. We note here that this fast relaxation occurs only between the exciton states in the same antenna units not between the exciton states of different antenna units.

Damjanović *et al.* [33] suggested that a weakly bound polaron can be formed in BChl aggregates due to the

² Another delocalized IS, which is the brightest exciton state of Roll B, shows the similar short time dynamics (see Set II and the Appendix for the corresponding time constants and the exciton dynamics, respectively).

interaction of excitons with intramolecular vibrational mode at about 1670cm^{-1} . Their results were based on studies of LHC in purple bacteria. We do expect that the polaron couplings can renormalize energy levels and the mobility of the exciton energy is reduced [33]. This should be, however, weaker in the chlorosome where BCHls are densely packed and the pigment-pigment interaction is, accordingly, stronger than that of LHC in purple bacteria.

The exciton dynamics in the FMOs is conditioned mainly by the population of the baseplate because direct population transfer from the roll to FMOs is negligible (see the Appendix).

B. Cooperativity of the excitonic states

In multichromophoric systems, coherent coupling between donor molecules can lead to a large collective transition dipole moment. This enhances the energy transfer from the donor to acceptor groups as compared to incoherent hopping between individual molecules [12, 14, 15, 90].

In Fig. 5, we show the cooperativity (Eq. 2) computed for first 500 fs. The cooperativity is calculated for the two different initial excitation conditions corresponding to the dynamics in Fig. 3.

The delocalized IS is z-polarized (along the length of the roll) and initially has a cooperativity of 402 (out of 1620 pigments in the Roll A). This strong collective oscillator strength can induce rapid supertransfer [12, 14, 15]. The localized IS, which is 72% x- and 28% z-polarized, has an initial cooperativity value of unity. This difference in cooperativity at varying initial condition is one of the reasons why a fast decay component is found for the delocalized IS case only.

Regardless of the initial conditions, within 500 fs, all cooperativity values converge to a similar value (~ 12 out of 3780 pigments in the Roll A and B), which is still larger than 1, and the effective transition dipole moment

Table I. **Time constants of the exciton dynamics of the chlorosome roll.** The values are obtained by the exponential fittings ($A_1 \exp(-t/\tau_1) + A_2 \exp(-t/\tau_2) + A_3 \exp(-t/\tau_3)$) of the exciton population dynamics for each antenna unit. The amplitudes (A_1 , A_2 and A_3) are summed to be 100%.

Set	τ_1 (ps)	(A_1 (%))	τ_2 (ps)	(A_2 (%))	τ_3 (ps)	(A_3 (%))
I ^a	0.081	(3)	4.5	(36)	12.9	(61)
II ^b	0.060	(3)	4.7	(39)	13.1	(58)
III ^c	-	-	3.7	(25)	11.3	(75)
Ref. [20] ^d	-	-	1.1	(42)	12.1	(58)

^a Corresponds to the exciton dynamics of the delocalized IS

^b Brightest delocalized initial state of Roll B is used. The exciton dynamics is given in the Appendix.

^c Corresponds to the exciton dynamics of the localized IS

^d Anisotropic decay of *Chlorobium tepidum* at 807 nm

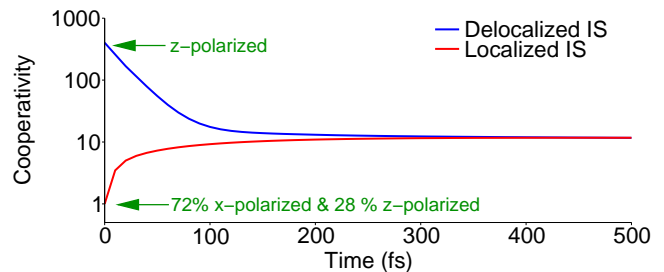


Figure 5. **Time dependent cooperativity of the chlorosome at 300 K.** The cooperativity (Eq. 2), dimensionless normalized collective transition dipole moment, is given in logarithmic scale. During the exciton dynamics in Fig. 3 with the two initial states, the cooperativities are calculated for the chlorosome.

becomes about 30% x-, 30% y- and 40% z-polarized. This is a favorable situation, for our photosynthetic apparatus model, as y-polarization (normal direction to the baseplate) is useful to funnel energy towards the baseplate. These results may indicate a multichromophoric effect [88]; *i.e.* the effective dipole moment of the delocalized exciton state is enhanced by symmetry (see also Ref. [91] for the discussion on the coherence and EET rate).

C. Temperature dependence of the energy funneling

In the previous subsections, we showed that the exciton energy funneling process is robust to variations in initial excitation conditions due to the fast internal exciton dynamics of the roll. We now investigate the temperature effect by simulating the exciton population dynamics with the delocalized IS initial condition, *i.e.* the brightest state of Roll A, at 150 K and 77 K in Fig. 6.

The mean exciton energy at room temperature (300 K) in Fig. 3A is only slightly different from the curves at 150 K and 77 K in Fig. 6. The corresponding exciton population dynamics are given in the Appendix. This indicates that exciton transfer is robust within this temperature range. The robust energy transfer within the temperature range is due to the fast internal exciton dynamics of the roll. The thermal excitation within the temperature range does not lift the exciton far from the energy resonance domain between the roll and the baseplate.

Thermal excitation in the temperature range (77, 150 and 300 K) can provide various channels towards the neighboring exciton states for the relaxation process (see Fig. 2B). Thermal excitation can also induce back transfer from the baseplate to the rolls [90] but it reduces the possibility of being trapped in dark states.

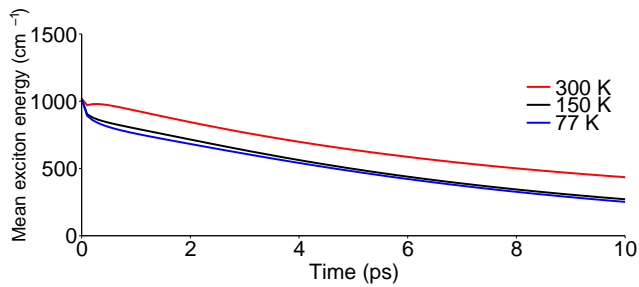


Figure 6. **Temperature dependence of the mean exciton energy.** The mean exciton energy of the system (Eq. 1) is plotted at 300 K, 150 K and 77 K. The delocalized exciton initial state in Fig. 3A is used.

D. Population kinetics

So far, we have shown that regardless of initial conditions and temperature about 60–70% of the exciton can be transferred to the FMOs within 10 ps. This robustness to the choice of initial conditions implies that internal dynamics within the roll is faster than energy transfer between the antenna units. We now proceed to examine the population dynamics by using a simple first order kinetic model (more sophisticated kinetic models in the EET of the LH complex networks can be found in *e.g.* Refs. [40, 41, 92, 93]):

$$\frac{d}{dt} \begin{pmatrix} [R](t) \\ [BP](t) \\ [FMO](t) \end{pmatrix} = \begin{pmatrix} -k_{RBP}(t) & 0 & 0 \\ k_{RBP}(t) & -k_{BPFMO}(t) & 0 \\ 0 & k_{BPFMO}(t) & 0 \end{pmatrix} \begin{pmatrix} [R](t) \\ [BP](t) \\ [FMO](t) \end{pmatrix} \quad (3)$$

where $[\cdot](t)$ denotes the population of each antenna unit, and $[R]$ and $[BP]$ are the population of the full roll (Roll A + Roll B) and the baseplate respectively. $k_{RBP}(t)$ is the exciton transfer rate from the roll to the baseplate and $k_{BPFMO}(t)$ is the one from the baseplate to the FMOs. The population transfer between the antenna units is characterized by time-dependent rate constants $k(t)$. Note that the internal dynamics within the antenna units, such as relaxation and thermal excitation among the exciton states, is incorporated into the time dependence of $k(t)$. $k(t)$, physically, corresponds to the multichromophoric Förster resonance energy transfer rate [88], because it quantifies energy transfer between the donor group (exciton states) of the roll and the acceptor group of the baseplate. The enhancement of energy transfer due to coherence (Fig. 5) between donor molecules is also referred as to supertransfer [12, 14, 15].

The direct exciton transfer from the roll to the FMO complexes is virtually negligible within the time interval of the EET dynamics 10 ps (see the Appendix). In this kinetic model, thus, we assume there is no population transfer from low to high energy units and no direct transfer from the roll to FMOs. The kinetic models are fitted to the exciton populations in Fig. 3 using least squares. The resulting time-dependent population trans-

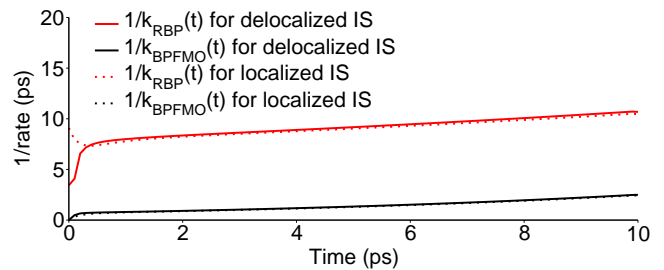


Figure 7. **Time dependent reciprocal rate.** Time-dependent exciton transfer rates are given as the corresponding time constants, the reciprocal rate, for the exciton dynamics of the delocalized IS and the localized IS in Fig. 3. $k_{RBP}(t)$: exciton transfer rate from the roll to the baseplate. $k_{BPFMO}(t)$: exciton transfer rate from the baseplate to the FMOs.

fer rates are shown in Fig. 7 for the exciton dynamics of Fig. 3, using both initial conditions (the delocalized IS and the localized IS). The initial and final values of the reciprocal rates of the (chlorosome) roll $1/k_{RBP}(t)$ have similar values to τ_2 and τ_3 of Sets I and III in Table I. Within 500 fs, $k_{RBP}(t)$ for the delocalized IS drops rapidly to a slower rate, with a similar timescale to the equilibrium time of the cooperativity (Eq. 2), see solid blue line in Fig. 5. However we see that $k_{RBP}(t)$ for the localized IS does not show this rapid drop. Regardless of the initial conditions, the rate constants become similar to each other within 500 fs. As could be expected, $k_{BPFMO}(t)$ has no dependence on the initial state in the roll.

III. CONCLUSION

The green sulfur bacteria are thought to be an incredibly efficient light processing machine (*cf.* purple bacterium in Ref. [94]). We studied this system by investigating from all-atoms and a top to bottom approach (*cf.* Ref. [95]). The excitation energy transfer route was taken from the chlorosome to the reaction center via the baseplate and FMO, under different initiating conditions. Analysis of the atomistic model indicates that resonant energy transfer is maximized given the multichromophoric excitonic coupling which is due to the molecular arrangements of these parts: the green sulfur bacteria are assembled to be most conducive towards efficient excitation energy transfer within the Förster energy transfer regime. It was further shown that whether the initial excitations are important in the energy funneling process. Though, the results differ qualitatively within a short time limit (500 fs). None of these scenario's, however, adversely affect the efficiency of energy transfer and the results converge within the overall timescale (10 ps) [20, 23]. Thus the mechanism is robust to initial conditions, including varying temperatures. This is due mainly to the fast internal exciton dynamics of the chlorosome, which is

also observed in Refs. [66, 96]. Furthermore our measure of cooperativity quantifies this and indicates a preference (again regardless of initial conditions) to the polarization in the xy-plane (cross section of the chlorosome), which enhances the excitonic coupling strengths between the exciton states of the chlorosome and the baseplate. We suggest a multichromophoric effect may prevail over the absence of proximity by exploiting the symmetry in parts of the model. This calculation of cooperativity indicates a supertransfer effect inherent in: the green sulfur bacteria, which seems to be especially “tuned” towards thriving under low light conditions by making use of molecular aggregates, symmetry and self-assembly to capture light and funnel it to the reaction center aided, not hindered, by a fluctuating environment [26, 97].

Additionally we would like to comment here on the role of the baseplate in the energy funneling process based on our simulations. In our model study, the baseplate plays the role of a “bridge” allowing the exciton energy to funnel down to the FMOs from the chlorosome. The presence of the baseplate eases this process; without the baseplate energy transfer would be impeded. Whilst it could be the case that transfer is allowed without the baseplate—under the condition that the FMO’s and chlorosomes be positioned close enough for Förster energy transfer—our results indicates that the baseplate offers a preferred route. The baseplate receives the exciton quickly as shown in Fig. 3 and releases the exciton to the FMO complexes steadily. Since the chlorosome has a relatively large reorganization energy, which implies strong exciton-phonon couplings to the bath, compared to those of the baseplate and FMO complexes, the exciton could be lost to the environment if it is able to stay in the chlorosome for too long a time. Thus, we would like to introduce the idea of the baseplate as a biological “exciton capacitor”. It seems to be suitably designed for this purpose, making sure the route of the exciton is directed, by receiving the exciton from the chlorosome quickly, keeping the exciton from leaking to the surrounding environment, and supplying it to the FMO. It does so by providing appropriate excitonic sites, via chromophoric pigments, held in a unique and protein scaffold made of amphiphilic units that cross two very different dielectric boundaries (the interim gap between dry lipid chlorosomes and the more watery region at the FMOs) in a near perfect 2D lattice form in analogy to an actual capacitor (condenser) but made of soft materials.

Our model study depends on many undetermined parameters, such as the site energies of the baseplate, distance between the antenna units and the spectral density of the baseplate. Also, the structure of the chlorosome is still arguable [48–54]. However, our study shows characteristic time constants that fall within sub-100 fs-sub-100 ps and agree with experimental observations [20, 23] (or see Table I).

ACKNOWLEDGMENTS

J. H. thanks Christoph Kreisbeck for the verification of numerical stability in the simulation and discussion about the spectral density. J. H., S. V., T. F. and A. A.-G. acknowledge support from the Center for Excitonics, an Energy Frontier Research Center funded by the US Department of Energy, Office of Science and Office of Basic Energy Sciences under award de-sc0001088. J. C. B. acknowledges support from Wellcome Trust UK. S. K. S. and A. A.-G. also acknowledge Defense Threat Reduction Agency grant HDTRA1-10-1-0046. Further, A. A.-G. is grateful for the support from Defense Advanced Research Projects Agency grant N66001-10-1-4063, and the Corning Foundation for their generous support.

Appendix A: Supporting Information

1. Method

Herein, the method that we use for the exciton propagation and computational details is presented.

Single exciton dynamics is described by Redfield quantum master equation (QME), which includes coherent, dephasing and relaxation processes [63, 68–71]. The complete system-bath Hamiltonian \hat{H} of the light-harvesting apparatus is composed of three parts, *i.e.* $\hat{H} = \hat{H}_S + \hat{H}_{SB} + \hat{H}_B$. \hat{H}_S is the system part of Hamiltonian, which describes the local excitations of N_S bacteriochlorophylls (BChls) and the interaction between them. The corresponding tight-binding Hamiltonian is given in a site basis $|m\rangle$ as,

$$\hat{H}_S = \sum_{m=1}^{N_S} \epsilon_m |m\rangle\langle m| + \sum_{n < m}^{N_S} V_{mn} (|m\rangle\langle n| + |n\rangle\langle m|), \quad (\text{A1})$$

where ϵ_m is a single excitation energy of the two-level system in site m and V_{mn} is the point dipole interaction energy between the site m and n . \hat{H}_{SB} is the linear coupling term between the system (BChls) and the bath (proteins) coordinate \hat{q}_m with a coupling strength k_m , *i.e.* $\hat{H}_{SB} = \sum_{m=1}^{N_S} k_m \hat{q}_m |m\rangle\langle m|$. \hat{H}_B is the bath Hamiltonian of multidimensional quantum harmonic oscillators. Within the secular (numerical degeneracy within 1 cm^{-1}) approximation and Markov limit, the Redfield QME of the (reduced) density operator $\hat{\rho}_S$ in the exciton basis is given as follow [68], for the diagonal and the off-diagonal elements, respectively,

$$\dot{\rho}_{S,KK}(t) = \sum_M (\gamma_{KM} \rho_{S,MM}(t) - \gamma_{MK} \rho_{S,KK}(t)), \quad (\text{A2})$$

$$\dot{\rho}_{S,KL}(t) = \left(-i\Delta E_{KL} + \gamma'_{KL} - \frac{1}{2} \sum_M (\gamma_{MK} + \gamma_{ML}) \right) \rho_{S,KL}(t), \quad (\text{A3})$$

where we additionally ignored the Lamb shift. \hat{H}_S^{EX} is the exciton Hamiltonian, which is in a diagonal form with the exciton eigenvalues E_M , that is $\hat{H}_S = \hat{C} \hat{H}_S^{\text{EX}} \hat{C}^\dagger$. γ_{MN} is the exciton transition rate between the corresponding exciton states $|M\rangle$ and $|N\rangle$. γ_{MN} is calculated with the exciton eigenvectors and spectral density $J_m(\Delta E_{MN}/\hbar)$ at the transition energy $\Delta E_{MN} = E_M - E_N$ and the

reciprocal temperature β (see Ref. [73] for the definition),

$$\gamma_{MN}(\frac{\Delta E_{MN}}{\hbar}; \beta) = \pi(1 + \coth(-\frac{\beta \Delta E_{MN}}{2})) \sum_m^{N_S} |C_{mM}|^2 |C_{mN}|^2 J_m(-\frac{\Delta E_{MN}}{\hbar}), \quad (\text{A4})$$

$$\gamma'_{MN}(\beta) = \frac{2\pi}{\beta} \sum_m^{N_S} |C_{mM}|^2 |C_{mN}|^2 \frac{dJ_m(\omega)}{d\omega} \Big|_{\omega=0}. \quad (\text{A5})$$

γ_{MN} satisfy the detailed balance condition, accordingly, $\gamma_{MN} = \gamma_{NM} \exp(\beta \Delta E_{MN})$.

2. Spectral density

We present the spectral densities we used in our simulations.

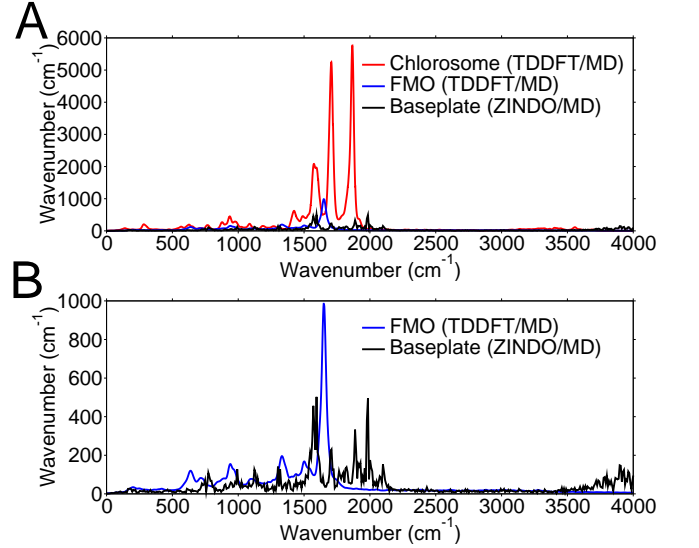


Figure A.1. **Spectral density.** **A.** Spectral densities were obtained individually for each photosynthetic unit from our previous works. The spectral density of the chlorosome (red line) and the FMO complexes (blue line) are collected from Fujita et al. [66] and Shim et al. [30]. We present here the spectral density of the baseplate obtained from ZINDO/MD calculations only to compare it with the spectral density of the FMO in the low frequency region. The ZINDO/MD spectral density of the baseplate is not used in the current work. Instead, we used the spectral density of the FMO complex as the one of the baseplate because we want to use spectral densities from the same methods. We note here again that the spectral densities are taken from the previous works [66, 73] not from the quantum mechanics / molecular mechanics calculations of the current model system (chlorosome+baseplate+FMO). **B.** The figure is magnified to compare the spectral densities of the baseplate and the FMO complex. We found that the spectral density of the baseplate is not too different from the one of FMO complex in the low frequency domain ($< 500 \text{ cm}^{-1}$), which is mainly responsible for the exciton transfer between the chlorosome and the baseplate.

3. Baseplate lattice model

We present the lattice model of the baseplate used in the current study.

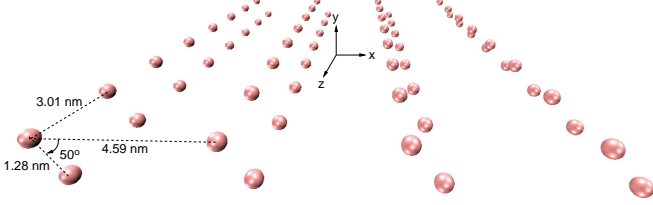


Figure A.2. **Baseplate lattice model.** The sphere represent the position of the Mg atom of the pigment. The lattice model has two layers. Each layer has 32 pigments. Two different transition dipole moments are used for the pigments in the different layers. The dipole moment vectors are $\mu_{top} = \sqrt{30}(0.2795, 0.7484, 0.5982)$ and $\mu_{bottom} = \sqrt{30}(0.2533, 0.1607, -0.9533)$, respectively for the top and bottom layers. The direction of the dipole moment is approximated by the N1-N3 vector of the BChls. y direction faces to the chlorosome and $-y$ does to the FMO complexes in the model.

4. Exciton dynamics

We present here the exciton dynamics, which are not shown in the article.

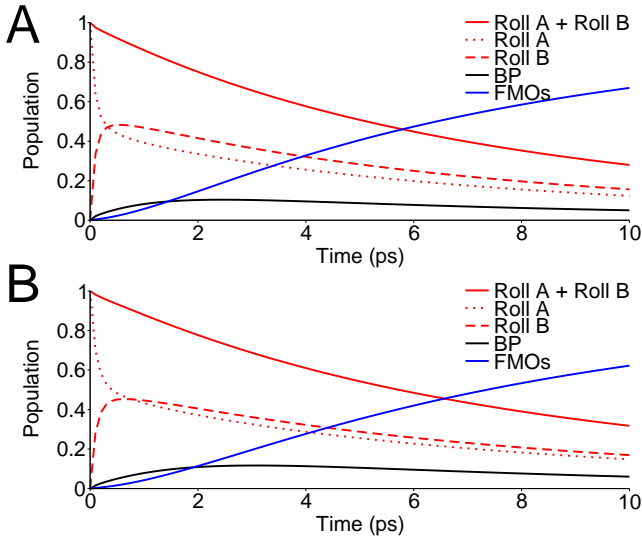


Figure A.3. **Exciton dynamics at 150 K and 77 K. A.** The exciton dynamics at 150 K with the brightest delocalized initial state of the Roll A. **B.** The exciton dynamics at 77 K with the brightest delocalized initial state of the Roll A.

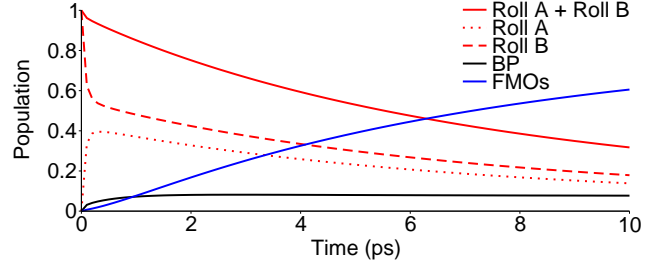


Figure A.4. **Exciton dynamics at 300 K with the brightest delocalized initial state of Roll B.** The exciton dynamics is obtained with the brightest delocalized initial state of Roll B.

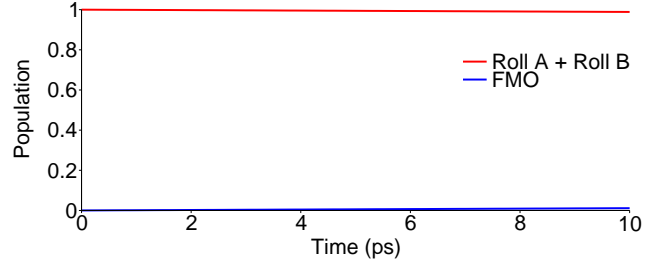


Figure A.5. **Exciton dynamics without the baseplate.** We test the exciton dynamics without the baseplate. The result is from a single trajectory calculation (the ensemble average is not taken).

5. Static disorder

Here, we present the effect of the static disorder.

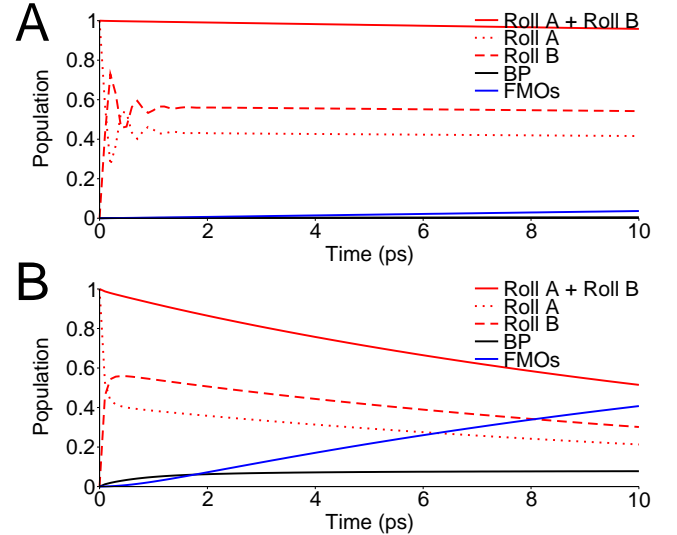


Figure A.6. **Exciton dynamics with and without the static disorder.** The dynamics were obtained at 300 K with the brightest delocalized initial state of the Roll A. **A.** The exciton dynamics without the static disorder. **B.** The exciton dynamics with the static disorder. The results are from single trajectory calculations (the ensemble average is not taken).

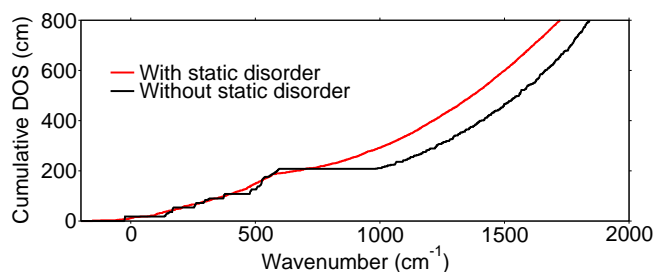


Figure A.7. **Cumulative density of states (DOS) with and without the static disorder.**

Cumulative-DOS(ω) = $\int_0^\omega d\omega \text{DOS}(\omega)$.

-
- [1] R. E. Blankenship, *Molecular Mechanisms of Photosynthesis*, World Scientific, 2002.
- [2] G. T. Oostergetel, H. van Amerongen, and E. J. Boekema, *The chlorosome: a prototype for efficient light harvesting in photosynthesis*, *Photosynth. Res.*, **104** (2010), pp. 245–55.
- [3] D. Canfield, B. Thamdrup, and E. Kristensen, *Aquatic geomicrobiology*, Elsevier, 2005.
- [4] J. Overmann, *The Prokaryotes. Volume 7: Proteobacteria: Delta, Epsilon Subclass*, eds. M. Dworkin, S. Falkow, E. Rosenberg, K.-H. Schleifer, and E. Stackebrandt, Springer, 2006, pp. 359–378.
- [5] X. Feng, K.-H. Tang, R. E. Blankenship, and Y. J. Tang, *Metabolic flux analysis of the mixotrophic metabolisms in the green sulfur bacterium Chlorobaculum tepidum*, *J. Bio. Chem.*, **285** (2010), pp. 39544–50.
- [6] J. Overmann, H. Cypionka, and N. Pfennig, *An extremely low-light-adapted phototrophic sulfur bacterium from the Black Sea*, *Limnol. Oceanog.*, **37** (1992), pp. 150–155.
- [7] J. T. Beatty, J. Overmann, M. T. Lince, A. K. Manske, A. S. Lang, R. E. Blankenship, C. L. Van Dover, T. A. Martinson, and F. G. Plumley, *An obligately photosynthetic bacterial anaerobe from a deep-sea hydrothermal vent*, *Proc. Natl. Acad. Sci.*, **102** (2005), pp. 9306–10.
- [8] A. K. Manske, J. Glaeser, M. M. M. Kuypers, and J. Overmann, *Physiology and Phylogeny of Green Sulfur Bacteria Forming a Monospecific Phototrophic Assemblage at a Depth of 100 Meters in the Black Sea*, *Physiology and Phylogeny of Green Sulfur Bacteria Forming a Monospecific Phototrophic Assemblage at a Depth of 100 M*, *Appl. Environ. Microbiol.*, **71** (2005), pp. 8049.
- [9] G. Engel, T. Calhoun, E. Read, T. Ahn, T. Mancal, Y. Cheng, R. Blankenship, and G. Fleming, *Evidence for wavelike energy transfer through quantum coherence in photosynthetic systems*, *Nature*, **446** (2007), pp. 782–786.
- [10] G. D. Scholes, G. R. Fleming, A. Olaya-Castro, and R. van Grondelle, *Lessons from nature about solar light harvesting*, *Nat. Chem.*, **3** (2011), pp. 763–74.
- [11] A. Borisov, *On the structure and function of chlorosomes of green bacteria*, *Biophysics*, **57** (2012), pp. 562–564.
- [12] S. Lloyd and M. Mohseni, *Symmetry-enhanced supertransfer of delocalized quantum states*, *New J. Phys.*, **12** (2010), pp. 075020.
- [13] S. Hoyer, M. Sarovar, and K. Birgitta Whaley, *Limits of quantum speedup in photosynthetic light harvesting*, *New J. Phys.*, **12** (2010), pp. 065041.
- [14] D. F. Abasto, M. Mohseni, S. Lloyd, and P. Zanardi, *Exciton diffusion length in complex quantum systems: the effects of disorder and environmental fluctuations on symmetry-enhanced supertransfer*, *Phil. Trans. R. Soc. A*, **370** (2013), pp. 3750–70.
- [15] I. Kassal, J. Yuen-Zhou, and S. Rahimi-Keshari, *Does Coherence Enhance Transport in Photosynthesis?*, *J. Phys. Chem. Lett.*, **4** (2013), pp. 362–367.
- [16] S. Savikhin, P. I. van Noort, Y. Zhu, S. Lin, R. E. Blankenship, and W. S. Struve, *Ultrafast energy transfer in light-harvesting chlorosomes from the green sulfur bacterium Chlorobium tepidum*, *Chem. Phys.*, **194** (1995), pp. 245–258.
- [17] J. Psencík, T. Polívka, J. Dian, J. Kudrna, and P. Malý, *Fast Energy Transfer and Exciton Dynamics in Chlorosomes of the Green Sulfur Bacterium Chlorobium tepidum*, *J. Phys. Chem. A*, **102** (1998), pp. 4392–4398.
- [18] V. I. Prokhorenko, D. B. Steensgaard, and A. R. Holzwarth, *Exciton dynamics in the chlorosomal antennae of the green bacteria Chloroflexus aurantiacus and Chlorobium tepidum*, *Biophys. J.*, **79** (2000), pp. 2105–20.
- [19] J. Psencík, Y.-Z. Ma, J. B. Arellano, J. Hála, and T. Gillbro, *Excitation energy transfer dynamics and excited-state structure in chlorosomes of Chlorobium phaeobacteroides*, *Biophys. J.*, **84** (2003), pp. 1161–79.
- [20] J. Martiskainen, J. Linnanto, V. Aumanen, P. Myllyperkiö, and J. Korppi-Tommola, *Excitation Energy Transfer in Isolated Chlorosomes from Chlorobaculum tepidum and Prosthecochloris aestuarii*, *Photochem. Photobiol.*, **88** (2012), pp. 675–683.
- [21] Z. Fetisova, a. Freiberg, K. Mauring, V. Novoderezhkin, a. Taisova, and K. Timpmann, *Excitation energy transfer in chlorosomes of green bacteria: theoretical and experimental studies*, *Biophys. J.*, **71** (1996), pp. 995–1010.
- [22] Y. Shibata, Y. Saga, H. Tamiaki, and S. Itoh, *Polarized fluorescence of aggregated bacteriochlorophyll c and baseplate bacteriochlorophyll a in single chlorosomes isolated from Chloroflexus aurantiacus*, *Biochemistry*, **46** (2007), pp. 7062–8.
- [23] J. Martiskainen, J. Linnanto, R. Kananavičius, V. Lehtovuori, and J. Korppi-Tommola, *Excitation energy transfer in isolated chlorosomes from Chloroflexus aurantiacus*, *Chem. Phys. Lett.*, **477** (2009), pp. 216–220.

- [24] K. Mukai, S. Abe, and H. Sumi, *Theory of Rapid Excitation-Energy Transfer from B800 to Optically-Forbidden Exciton States of B850 in the Antenna System LH2 of Photosynthetic Purple Bacteria*, *J. Phys. Chem. B*, **103** (1999), pp. 6096–6102.
- [25] S. Jang, M. D. Newton, and R. J. Silbey, *Multichromophoric Förster resonance energy transfer from b800 to b850 in the light harvesting complex 2: evidence for subtle energetic optimization by purple bacteria*, *J. Phys. Chem. B*, **111** (2007), pp. 6807–14.
- [26] M. Mohseni, P. Rebentrost, S. Lloyd, and A. Aspuru-Guzik, *Environment-assisted quantum walks in photosynthetic energy transfer*, *J. Chem. Phys.*, **129** (2008), pp. 174106.
- [27] A. Ishizaki and G. R. Fleming, *Theoretical examination of quantum coherence in a photosynthetic system at physiological temperature*, *Proc. Natl. Acad. Sci.*, **106** (2009), pp. 17255–60.
- [28] J. Strümpfer and K. Schulten, *Light Harvesting complex II B850 excitation dynamics*, *J. Chem. Phys.*, **131** (2009), pp. 225101.
- [29] G. Ritschel, J. Roden, W. T. Strunz, A. Aspuru-Guzik, and A. Eisfeld, *Absence of Quantum Oscillations and Dependence on Site Energies in Electronic Excitation Transfer in the Fenna-Matthews-Olson Trimer*, *J. Phys. Chem. Lett.*, **2** (2011), pp. 2912–2917.
- [30] S. Shim, P. Rebentrost, S. Valleau, and A. Aspuru-Guzik, *Atomistic study of the long-lived quantum coherences in the Fenna-Matthews-Olson complex*, *Biophys. J.*, **102** (2012), pp. 649–60.
- [31] C. Kreisbeck and T. Kramer, *Long-Lived Electronic Coherence in Dissipative Exciton Dynamics of Light-Harvesting Complexes*, *J. Phys. Chem. Lett.*, **3** (2012), pp. 2828–2833.
- [32] H. W. Kim, A. Kelly, J. W. Park, and Y. M. Rhee, *All-atom semiclassical dynamics study of quantum coherence in photosynthetic Fenna-Matthews-Olson complex*, *J. Am. Chem. Soc.*, **134** (2012), pp. 11640–51.
- [33] A. Damjanović, I. Kosztin, U. Kleinekathöfer, and K. Schulten, *Excitons in a photosynthetic light-harvesting system: A combined molecular dynamics, quantum chemistry, and polaron model study*, *Phys. Rev. E*, **65** (2002), pp. 1–24.
- [34] C. Olbrich and U. Kleinekathöfer, *Time-dependent atomistic view on the electronic relaxation in light-harvesting system II*, *J. Phys. Chem. B*, **114** (2010), pp. 12427–37.
- [35] X. Hu, T. Ritz, A. Damjanovic, and K. Schulten, *Pigment Organization and Transfer of Electronic Excitation in the Photosynthetic Unit of Purple Bacteria*, *J. Phys. Chem. B*, **101** (1997), pp. 3854–3871.
- [36] M. K. Sener, J. D. Olsen, C. N. Hunter, and K. Schulten, *Atomic-level structural and functional model of a bacterial photosynthetic membrane vesicle*, *Proc. Natl. Acad. Sci.*, **104** (2007), pp. 15723–8.
- [37] A. Olaya-Castro, C. Lee, F. Olsen, and N. Johnson, *Efficiency of energy transfer in a light-harvesting system under quantum coherence*, *Phys. Rev. B*, **78** (2008), pp. 085115.
- [38] A. K. Ringsmuth, G. J. Milburn, and T. M. Stace, *Multiscale photosynthetic and biomimetic excitation energy transfer*, *Nat. Phys.*, **8** (2012), pp. 562–567.
- [39] J. Dostál, T. Mančal, R. Augulis, F. Vácha, J. Pšenčík, and D. Zigmantas, *Two-dimensional electronic spectroscopy reveals ultrafast energy diffusion in chlorosomes*, *J. Am. Chem. Soc.*, **134** (2012), pp. 11611–7.
- [40] J. Cao and R. J. Silbey, *Optimization of exciton trapping in energy transfer processes*, *J. Phys. Chem. A*, **113** (2009), pp. 13825–38.
- [41] F. Caruso, A. W. Chin, A. Datta, S. F. Huelga, and M. B. Plenio, *Highly efficient energy excitation transfer in light-harvesting complexes: The fundamental role of noise-assisted transport*, *J. Chem. Phys.*, **131** (2009), pp. 105106.
- [42] M. O. Pedersen, J. Linnanto, N.-U. Frigaard, N. C. Nielsen, and M. Miller, *A model of the protein-pigment baseplate complex in chlorosomes of photosynthetic green bacteria*, *Photosynth. Res.*, **104** (2010), pp. 233–43.
- [43] J. M. Olson, *The FMO Protein*, *Photosynth. Res.*, **80** (2004), pp. 181–187.
- [44] F. Förster, *Zwischenmolekulare Energiewanderung und Fluoreszenz*, *Ann. Phys.*, **437** (1948), pp. 55–75.
- [45] V. May and O. Kühn, *Charge and Energy Transfer Dynamics in Molecular Systems*, Wiley-VCH, 2011, 3rd edition.
- [46] E. N. Zimanyi and R. J. Silbey, *Theoretical description of quantum effects in multi-chromophoric aggregates*, *Phil. Trans. R. Soc. A*, **370** (2012), pp. 3620–37.
- [47] N.-U. Frigaard, A. G. M. Chew, H. Li, J. A. Maresca, and D. A. Bryant, *Chlorobium tepidum: insights into the structure, physiology, and metabolism of a green sulfur bacterium derived from the complete genome sequence*, *Photosynth. Res.*, **78** (2003), pp. 93–117.
- [48] A. R. Holzwarth and K. Schaffner, *On the structure of bacteriochlorophyll molecular aggregates in the chlorosomes of green bacteria. A molecular modelling study*, *Photosynth. Res.*, **41** (1994), pp. 225–233.
- [49] R. Frese, U. Oberheide, I. V. Stokkum, R. V. Grondelle, M. Foidl, and H. V. Amerongen, *The organization of bacteriochlorophyll c in chlorosomes from Chloroflexus aurantiacus and the structural role of carotenoids and protein An absorption , linear dichroism , circular dichroism and Stark spectroscopy study*, *Photosynth. Res.*, **54** (1997), pp. 115–126.
- [50] J. Psencík, T. P. Ikonen, P. Laurinmäki, M. C. Merckel, S. J. Butcher, R. E. Serimaa, and R. Tuma, *Lamellar organization of pigments in chlorosomes, the light harvesting complexes of green photosynthetic bacteria*, *Biophys. J.*, **87** (2004), pp. 1165–1172.
- [51] J. M. Linnanto and J. E. I. Korppi-Tommola, *Investigation on chlorosomal antenna geometries: tube, lamella and spiral-type self-aggregates*, *Photosynth. Res.*, **96** (2008), pp. 227–45.
- [52] S. Ganapathy, G. T. Oostergetel, P. K. Wawrzyniak, M. Reus, A. Gomez Maqueo Chew, F. Buda, E. J. Boekema, D. A. Bryant, A. R. Holzwarth, and H. J. M. de Groot, *Alternating syn-anti bacteriochlorophylls form concentric helical nanotubes in chlorosomes*, *Proc. Natl. Acad. Sci.*, **106** (2009), pp. 8525–30.
- [53] S. Ganapathy, G. T. Oostergetel, M. Reus, Y. Tsukatani, A. Gomez Maqueo Chew, F. Buda, D. A. Bryant, A. R. Holzwarth, and H. J. de Groot, *Structural variability in wild-type and bchQ bchR mutant chlorosomes of the green sulfur bacterium Chlorobaculum tepidum.*, *Biochemistry*, **51** (2012), pp. 4488–98.
- [54] J. K.-H. Tang, S. K. Saikin, S. V. Pingali, M. M. Enriquez, J. Huh, H. A. Frank, V. S. Urban, and A. Aspuru-Guzik, *Temperature and Carbon Assimilation Regulate the Chlorosome Biogenesis in Green Sulfur Bacteria*,

- arXiv:1307.1742, (2013).
- [55] Y. Tian, R. Camacho, D. Thomsson, M. Reus, A. R. Holzwarth, and I. G. Scheblykin, *Organization of bacteriochlorophylls in individual chlorosomes from Chlorobaculum tepidum studied by 2-dimensional polarization fluorescence microscopy*, J. Am. Chem. Soc., **133** (2011), pp. 17192–9.
- [56] M. O. S. Pedersen, J. Underhaug, J. Dittmer, M. Miller, and N. C. Nielsen, *The three-dimensional structure of CsmA: a small antenna protein from the green sulfur bacterium Chlorobium tepidum*, FEBS letters, **582** (2008), pp. 2869–74.
- [57] J. Phillips, R. Braun, W. Wang, J. Gumbart, E. Tajkhorshid, E. Villa, C. Chipot, R. Skeel, L. Kale, and K. Schulten, *Scalable molecular dynamics with NAMD*, J. Comput. Chem., **26** (2005), pp. 1781–1802.
- [58] V. Hornak, R. Abel, A. Okur, B. Strockbine, A. Roitberg, and C. Simmerling, *Comparison of multiple Amber force fields and development of improved protein backbone parameters*, Proteins, **65** (2006), pp. 712–25.
- [59] R. E. Blankenship, M. T. Madigan, and C. E. Bauer, *Anoxygenic photosynthetic bacteria*, Kluwer Academic Publishers, 1995.
- [60] D. E. Tronrud, J. Wen, L. Gay, and R. E. Blankenship, *The structural basis for the difference in absorbance spectra for the FMO antenna protein from various green sulfur bacteria*, Photosynth. Res., **100** (2009), pp. 79–87.
- [61] J. Wen, H. Zhang, M. L. Gross, and R. E. Blankenship, *Membrane orientation of the FMO antenna protein from Chlorobaculum tepidum as determined by mass spectrometry-based footprinting*, Proc. Natl. Acad. Sci., **106** (2009), pp. 6134–9.
- [62] M. Schmidt am Busch, F. Müh, M. El-Amine Madjet, and T. Renger, *The Eighth Bacteriochlorophyll Completes the Excitation Energy Funnel in the FMO Protein*, J. Phys. Chem. Lett., **2** (2011), pp. 93–98.
- [63] J. Adolphs and T. Renger, *How proteins trigger excitation energy transfer in the FMO complex of green sulfur bacteria*, Biophys. J., **91** (2006), pp. 2778–97.
- [64] M. T. W. Milder, B. Brüggemann, R. van Grondelle, and J. L. Herek, *Revisiting the optical properties of the FMO protein*, Photosynth. Res., **104** (2010), pp. 257–74.
- [65] C. Francke and J. Ames, *Isolation and pigment composition of the antenna system of four species of green sulfur bacteria*, Photosynth. Res., (1997), pp. 137–146.
- [66] T. Fujita, J. C. Brookes, S. K. Saikin, and A. Aspuru-Guzik, *Memory-Assisted Exciton Diffusion in the Chlorosome Light-Harvesting Antenna of Green Sulfur Bacteria*, J Phys. Chem. Lett., **3** (2012), pp. 2357–2361.
- [67] V. I. Prokhorenko, D. B. Steensgaard, and A. R. Holzwarth, *Exciton theory for supramolecular chlorosomal aggregates: 1. Aggregate size dependence of the linear spectra*, Biophys. J., **85** (2003), pp. 3173–86.
- [68] W. H. Louisell, *Quantum Statistical Properties of Radiation*, John Wiley & Sons, 1973.
- [69] H. P. Breuer and F. Petruccione, *The Theory of Open Quantum Systems*, Oxford University, 2006.
- [70] P. Rebentrost, R. Chakraborty, and A. Aspuru-Guzik, *Non-Markovian quantum jumps in excitonic energy transfer*, J. Chem. Phys., **131** (2009), pp. 184102.
- [71] P. Rebentrost, M. Mohseni, and A. Aspuru-Guzik, *Role of quantum coherence and environmental fluctuations in chromophoric energy transport*, J. Phys. Chem. B, **113** (2009), pp. 9942–7.
- [72] A. Ishizaki and G. R. Fleming, *On the adequacy of the Redfield equation and related approaches to the study of quantum dynamics in electronic energy transfer*, J. Chem. Phys., **130** (2009), pp. 234110.
- [73] S. Valleau, A. Eisfeld, and A. Aspuru-Guzik, *On the alternatives for bath correlators and spectral densities from mixed quantum-classical simulations*, J. Chem. Phys., **137** (2012), pp. 224103.
- [74] W. M. Zhang, T. Meier, V. Chernyak, and S. Mukamel, *Exciton-migration and three-pulse femtosecond optical spectroscopies of photosynthetic antenna complexes of photosynthetic antenna complexes*, J. Chem. Phys., **108** (1998), pp. 7763.
- [75] T. Pullerits, *Exciton States and Relaxation in Molecular Aggregates: Numerical Study of Photosynthetic Light Harvesting*, J. Chin. Chem. Soc., **47** (2000), pp. 773–784.
- [76] M. Yang and G. R. Fleming, *Influence of phonons on exciton transfer dynamics: comparison of the Redfield, Förster and modified Redfield equations*, Chem. Phys., **275** (2002), pp. 355–372.
- [77] V. Novoderezhkin, J. M. Salverda, and H. V. Amerongen, *Exciton Modeling of Energy-Transfer Dynamics in the LHCII Complex of Higher Plants: A Redfield Theory Approach*, J. Phys. Chem. B, (2003), pp. 1893–1912.
- [78] V. I. Novoderezhkin, M. A. Palacios, and H. V. Amerongen, *Energy-Transfer Dynamics in the LHCII Complex of Higher Plants: Modified Redfield*, J. Phys. Chem. B, (2004), pp. 10363–10375.
- [79] A. Ishizaki and G. R. Fleming, *Unified treatment of quantum coherent and incoherent hopping dynamics in electronic energy transfer: reduced hierarchy equation approach*, J. Chem. Phys., **130** (2009), pp. 234111.
- [80] C. Kreisbeck, T. Kramer, M. Rodríguez, and B. Hein, *High-Performance Solution of Hierarchical Equations of Motion for Studying Energy Transfer in Light-Harvesting Complexes*, J. Chem. Theory Comput., **7** (2011), pp. 2166–2174.
- [81] J. Zhu, S. Kais, P. Rebentrost, and A. Aspuru-Guzik, *Modified scaled hierarchical equation of motion approach for the study of quantum coherence in photosynthetic complexes*, J. Phys. Chem. B, **115** (2011), pp. 1531–7.
- [82] P. Huo and D. F. Coker, *Theoretical Study of Coherent Excitation Energy Transfer in Cryptophyte Phycocyanin 645 at Physiological Temperature*, J. Phys. Chem. Lett., **2** (2011), pp. 825–833.
- [83] G. Ritschel, J. Roden, W. T. Strunz, and A. Eisfeld, *An efficient method to calculate excitation energy transfer in light-harvesting systems: application to the Fenna-Matthews-Olson complex*, New J. Phys., **13** (2011), pp. 113034.
- [84] D. P. S. Mccutcheon and A. Nazir, *Consistent treatment of coherent and incoherent energy transfer dynamics using a variational master equation*, J. Chem. Phys., **135** (2011), pp. 114501.
- [85] L. Mühlbacher and U. Kleinekathöfer, *Preparational effects on the excitation energy transfer in the FMO complex*, J. Phys. Chem. B, **116** (2012), pp. 3900–6.
- [86] L. A. Pachón and P. Brumer, *Computational methodologies and physical insights into electronic energy transfer in photosynthetic light-harvesting complexes*, Phys. Chem. Chem. Phys., **14** (2012), pp. 10094–108.
- [87] P. Brumer and M. Shapiro, *Molecular response in one-photon absorption via natural thermal light vs. pulsed laser excitation*, Proc. Natl. Acad. Sci., **109** (2012), pp.

- 19575–8.
- [88] S. Jang, M. Newton, and R. Silbey, *Multichromophoric Förster Resonance Energy Transfer*, Phys. Rev. Lett., **92** (2004), pp. 218301–4.
- [89] J. Roden, G. Schulz, A. Eisfeld, and J. Briggs, *Electronic energy transfer on a vibronically coupled quantum aggregate.*, J. Chem. Phys., **131** (2009), pp. 044909.
- [90] T. P. Causgrove, D. C. Brune, and R. E. Blankenship, *Förster energy transfer in chlorosomes of green photosynthetic bacteria*, J. Photochem. Photobiol. B: Biol., **15** (1992), pp. 171–9.
- [91] J. Strümpfer, M. Sener, and K. Schulten, *How Quantum Coherence Assists Photosynthetic Light Harvesting*, J. Phys. Chem. Lett., **3** (2012), pp. 536–542.
- [92] M. Yang and G. R. Fleming, *Construction of kinetic domains in energy trapping processes and application to a photosynthetic light harvesting complex*, J. Chem. Phys., **119** (2003), pp. 5614.
- [93] L. Valkunas, J. Chmeliov, G. Trinkunas, C. D. P. Duffy, R. van Grondelle, and A. V. Ruban, *Excitation migration, quenching, and regulation of photosynthetic light harvesting in photosystem II*, J. Phys. Chem. B, **115** (2011), pp. 9252–60.
- [94] R. Hildner, D. Brinks, J. B. Nieder, R. J. Cogdell, and N. F. van Hulst, *Quantum Coherent Energy Transfer over Varying Pathways in Single Light-Harvesting Complexes*, Science, **340** (2013), pp. 1448–1451.
- [95] J. M. Linnanto and J. E. I. Korppi-tommola, *Exciton Description of Chlorosome to Baseplate Excitation Energy Transfer in Filamentous Anoxygenic Phototrophs and Green Sulfur Bacteria*, J. Phys. Chem. B, **117** (2013), pp. 11144–11161.
- [96] T. Fujita, J. Huh, S. K. Saikin, J. C. Brookes, and A. Aspuru-Guzik, *Theoretical characterization of excitation energy transfer in chlorosome light-harvesting antennae from green sulfur bacteria*, arXiv:1304.4902v2, (2013).
- [97] P. Reberstrost, M. Mohseni, I. Kassal, S. Lloyd, and A. Aspuru-Guzik, *Environment-assisted quantum transport*, New J. Phys., **11** (2009), pp. 033003.